Observation of vector solitary waves in soft laminates using designated finite volume method

Ron Ziv and Gal Shmuel*

Faculty of Mechanical Engineering, Technion–Israel Institute of Technology, Haifa 32000, Israel

Abstract

Soft materials with engineered microstructure support nonlinear waves which can be harnessed for various applications, from signal communication to impact mitigation. Such waves are governed by nonlinear coupled differential equations whose analytical solution is seldom trackable, hence emerges the need for suitable numerical solvers. Based on the finite volume method, we here develop the first designated scheme for nonlinear waves with two coupled components that propagate in soft laminates. We apply our scheme to a periodic laminate made of two alternating Gent layers, and consider two cases. In one case, we analyze a motion whose component along the lamination direction is coupled to a component in the layers plane, to discover the first vector solitary waves in a continuum medium. In the second case, we analyze a motion with two coupled components in the plane of the layers, and observe the propagation of linearly polarized solitary waves, followed by a single circularly polarized wave. The framework we developed offers a platform for further investigation of these waves and their extension to higher dimensional problems.

Keywords: finite volume method, composites, laminates, soft materials, nonlinear elasticity, finite deformations, wave propagation, solitary waves, Gent material

1 Introduction

Highly deformable materials with architectured microstructure are nowadays accessible by virtue of the current manufacturing abilities. Such materials exhibit geometrical and constitutive nonlinearities that give rise to fascinating physics (Bertoldi et al., 2017), and specifically unique wave phenomena (Nadkarni et al., 2014, 2016, Samsonov et al., 2017, Ziv and Shmuel, 2019a, Deng

*Corresponding author. Tel.: +1 972 778871613. *E-mail address*: meshmuel@technion.ac.il (G. Shmuel).

et al., 2019a). Waves in nonlinear solids have recently regained scientific and technological interest, owing to the realization that their features can be harnessed for various applications, such as signal transmission (Raney et al., 2016), impact mitigation (Yasuda et al., 2019), energy harvesting (Hwang and Arrieta, 2018) and mechanical diodes (Deng et al., 2018).

The mathematical modeling of waves in soft solids with microstructure is given by nonlinear coupled partial differential equations, whose analytical solution is seldom trackable (Carroll, 1967, Davison, 1966, Destrade and Saccomandi, 2005, Chockalingam and Cohen, 2020), hence the need for designated numerical solvers. Among the different schemes developed for nonlinear elastodynamics, we recall the finite difference method (Aboudi and Benveniste, 1973), finite element method (Bou Matar et al., 2012, Chabot et al., 2018), and specifically the finite volume method (LeVeque, 1992, Tripathi et al., 2019).

Finite volume methods are useful in solving problems whose physics is governed by space-time conservation laws, and as such are useful in gas dynamics (Roe, 1985) and elastodynamics (LeVeque, 1997). Importantly, these methods are conservative in the sense that by construction they satisfy the conservation law in an exact manner—a useful feature in problems whose solution is discontinuous (Lax and Wendroff, 1960). Further, since the method is based on flux terms that are evaluated at the boundary of volume elements, it naturally lends itself to the analysis of heterogeneous layered media–where suitable continuity conditions are to be satisfied at the boundaries between different layers. Indeed, the efficiency of the finite volume approach was demonstrated by Fogarty and LeVeque (1999), who developed a finite volume scheme for one-dimensional waves in linear elastic laminates, and later on by LeVeque (2002), who extended the analysis to nonlinear laminates. More recent works have further developed this approach for additional problems, *e.g.*, materials that exhibit softening (Berjamin et al., 2019), elastoplastic materials (Barton et al., 2010), and thermoelastic materials (Berezovski and Maugin, 2001), to name a few.

To date, a finite volume scheme for nonlinear heterogeneous media exhibiting coupled motions has yet to be formulated. Here, we develop such a scheme for composites made of soft layers, when subjected to time-dependent deformations comprising two coupled components. Specifically, we consider one case where the component of the deformation in the lamination direction (referred to as the axial component) is coupled with a transverse component in the plane of the layers (Davison, 1966), and a second case where two components in the layers plane are coupled one with the other (Collins, 1966). Our method builds upon the finite volume approach of LeVeque (2002), who utilizes solutions for *Riemann problems*—problems of wave scattering owing to discontinuous initial conditions and possibly different materials—to calculate one-dimensional waves in nonlinear laminates. Since that benchmark problem considers one component of motion, two waves of opposite propagation direction are generated at each scattering; here, two coupled components are present, hence four coupled waves are generated—two in each direction. Our extension accounts

for the generation of these additional waves and their coupling, by the development of a suitable matrix representation. Further, our scheme incorporates a *wave limiter* (LeVeque, 1997)—a scalar function aimed at limiting the gradient of the solution near discontinuities—which proves useful in capturing shock waves.

We validate our method by applying it for the canonical problem of wave scattering at an interface between two elastic half-spaces. The aspect of shock evaluation in this setting was addressed by Davison (2008), who studied axial waves. Here, we extend the analysis to shocks associated with waves comprising two coupled components, noting that this is the first study of such problems. Specifically, we compare our finite volume-based solution to the linearized algebraic equations with numerical solutions using Newton's method to the exact nonlinear equations, when the media is governed by the compressible Gent model (Gent, 1996). This model—originally developed for capturing the strain stiffening of rubber at large strains—was recently shown useful by Ziv and Shmuel (2019a) for modeling shear shocks and tensile-induced shocks (Niemczura and Ravi-Chandar, 2011, Catheline et al., 2003, Espíndola et al., 2017, Espindola and Pinton, 2017). We find an excellent agreement between our scheme and Newton's method, particularly at material interfaces, and demonstrate the merit of a wave limiter in capturing discontinuities in the solution.

Subsequently, we apply our scheme to a pre-strained laminate made of two alternating Gentian layers. Remarkably, in the case where the axial and transverse components of the motion are coupled, our numerical solution reveals a generation of elastic vector solitary waves—nonlinear waves having two coupled components of constant shape and velocity. Our results are thus the first report of a continuum analog of the vector solitary waves observed recently in discrete media (Deng et al., 2017, 2018, 2019b). Furthermore, in the case where the coupling is between two transverse components, we discover the propagation of linearly polarized solitary waves, followed by a single circularly polarized wave.

Our results are presented in the following order. Sec. 2 summarizes the equations governing motions with two coupled components in laminates made of nonlinear layers, and Sec. 3 details our finite volume method for the solution of these equations. We apply our method in Sec. 4 to coupled waves in Gentian layers, where we also report the corresponding propagation of vector solitary waves and linearly polarized solitary waves. We summarize our main results and conclusions in Sec. 5, together with an outlook towards future work.

2 Governing equations

We consider a soft composite made of N hyperelastic phases that are laminated in the X_1 direction. We denote the initial mass density and strain energy density function of phase n by $\rho_L^{(n)}$ and $\Psi^{(n)}$. Phase n initially occupies the region $\Omega^{(n)}$, and accordingly the energy density function of the

composite, $\Psi(\mathbf{F},\mathbf{X})$, is

$$\Psi(\mathbf{F},\mathbf{X}) = \sum_{n=1}^{N} \mathbb{1}^{(n)}(\mathbf{X})\,\Psi^{(n)}(\mathbf{F}), \tag{1}$$

where

$$\mathbb{1}^{(n)}(\mathbf{X}) = \begin{cases} 1 & \mathbf{X} \in \Omega^{(n)}, \\ 0 & \text{elsewhere.} \end{cases} \tag{2}$$

The composite is subjected to the motion $\chi(\mathbf{X},t)$

$$x_1 = X_1 + u_1(X_1,t),\ x_2 = X_2 + u_2(X_1,t),\ x_3 = X_3 + u_3(X_1,t), \tag{3}$$

which maps material points from the reference coordinate $\mathbf{X}$ to the current coordinate $\mathbf{x}$. The resultant first Piola-Kirchhoff stress tensor is $\mathbf{P} = \nabla_{\mathbf{F}}\Psi$, where $\mathbf{F}=\nabla_{\mathbf{X}}\chi$ is the deformation gradient. We assume that the phases are initially isotropic, and hence $\mathbf{P}$ has the form

$$\mathbf{P} = \alpha_1\mathbf{F} + \alpha_2\mathbf{F}\mathbf{F}^{\mathrm{T}}\mathbf{F} + \alpha_3\mathbf{F}^{-\mathrm{T}} \tag{4}$$

for some response functions α_i. The Lagrangian equations of motion are

$$\nabla_{\mathbf{X}} \cdot \mathbf{P} = \rho_L \chi_{,tt}, \tag{5}$$

where we tacitly assume that χ is continuous and twice differentiable (except at material interfaces). For the mapping of interest (3), Eq. (5) reduces to

$$P_{i1,1} = \rho_L \frac{\partial^2 u_i}{\partial t^2},\ i = 1,2,3. \tag{6}$$

Focusing on motions in which either $u_1 \equiv 0$ or $u_3 \equiv 0$, we rewrite Eq. (6) as

$$u_1 \equiv 0:\ P_{21,1} = \rho_L \frac{\partial^2 u_2}{\partial t^2}\ ,\ P_{31,1} = \rho_L \frac{\partial^2 u_3}{\partial t^2}; \tag{7a,b}$$

$$u_3 \equiv 0:\ P_{11,1} = \rho_L \frac{\partial^2 u_1}{\partial t^2}\ ,\ P_{21,1} = \rho_L \frac{\partial^2 u_2}{\partial t^2}. \tag{7c,d}$$

Physically, $u_1 \equiv 0$ corresponds to transverse motion in the plane perpendicular to X_1 (Fig. 1b), whereas $u_3 \equiv 0$ corresponds to coupled axial and transverse motions (Fig. 1c). We can analyze the two cases together using a unifying equation by replacing the first index of $\mathbf{P}$ in Eqs. (7a) and (7c) by a and in Eqs. (7b) and (7d) by b, and writing

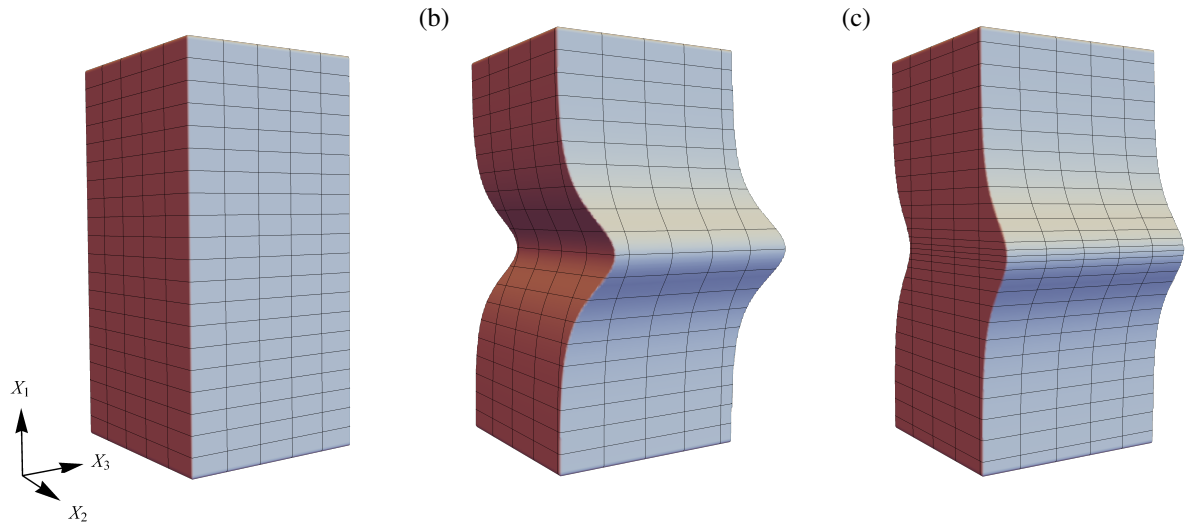

Figure 1: (a) Reference configuration of a representative phase. (b) Illustrative deformation when $u_1 \equiv 0$, and (c) $u_3 \equiv 0$.

$$P_{a1,1} = \rho_L \frac{\partial^2 u_a}{\partial t^2},\ P_{b1,1} = \rho_L \frac{\partial^2 u_b}{\partial t^2}. \tag{8}$$

We denote the spatial and temporal derivatives of u_i by

$$\varepsilon_i := \frac{\partial u_i}{\partial X_1},\ v_i := \frac{\partial u_i}{\partial t},\ i = a,b, \tag{9}$$

and put Eq. (8) in the form

$$\begin{pmatrix} \varepsilon_a \\ \varepsilon_b \\ \rho_L v_a \\ \rho_L v_b \end{pmatrix}_{,t} + \begin{pmatrix} -v_a \\ -v_b \\ -P_{a1} \\ -P_{b1} \end{pmatrix}_{,X_1} = \begin{pmatrix} 0 \\ 0 \\ 0 \\ 0 \end{pmatrix}, \tag{10}$$

which is reminiscent of a conservation equation for the left column. By applying the chain rule, we obtain

$$\begin{pmatrix} \varepsilon_a \\ \varepsilon_b \\ \rho_L v_a \\ \rho_L v_b \end{pmatrix}_{,t} + \begin{pmatrix} 0 & 0 & -\frac{1}{\rho_L} & 0 \\ 0 & 0 & 0 & -\frac{1}{\rho_L} \\ -\alpha & -\beta & 0 & 0 \\ -\gamma & -\delta & 0 & 0 \end{pmatrix} \begin{pmatrix} \varepsilon_a \\ \varepsilon_b \\ \rho_L v_a \\ \rho_L v_b \end{pmatrix}_{,X_1} = \begin{pmatrix} 0 \\ 0 \\ 0 \\ 0 \end{pmatrix}, \tag{11}$$

where

$$\alpha = \frac{\partial P_{a1}}{\partial \varepsilon_a},\ \beta = \frac{\partial P_{a1}}{\partial \varepsilon_b},\ \gamma = \frac{\partial P_{b1}}{\partial \varepsilon_a},\ \delta = \frac{\partial P_{b1}}{\partial \varepsilon_b}. \tag{12}$$

The eigenvalues of Eq. (11) are the following characteristic wave velocities in the material

$$c = \pm\sqrt{\frac{1}{2\rho_L}\left[\alpha+\delta \pm \sqrt{(\alpha-\delta)^2+4\beta\gamma}\right]} =: \pm c_\pm, \tag{13}$$

where c_+ and c_- correspond to the plus and minus sign of the inner square root, respectively. In the limit of linear elasticity, c_- and c_+ associated with Eq. (7c,d) governing coexisting transverse and axial motions correspond to the velocities of shear and pressure waves, respectively.

Collins (1966) showed that coupled transverse deformations with finite amplitude associated with Eq. (7a,b) generally propagate as a combination of circularly polarized waves with the velocity c_- and linearly polarized waves with the velocity c_+. This nature of motion is revealed using the transformation $\varepsilon_2 = \varepsilon_T \cos\theta$ and $\varepsilon_3 = \varepsilon_T \sin\theta$, which decouples the waves such that ε_T and θ are constants across waves propagating with the velocities c_- and c_+, respectively.

In the subsequent sections we formulate a finite volume method for layered materials governed by Eq. (11), and implement it for two fundamental problems of interest.

3 Finite volume method for waves with two coupled components

A finite volume method for waves with a single component was developed by LeVeque (1997, 2002). In this section, we generalize his method to waves comprising two coupled components, governed by equations in the form of Eq. (11).

We define the medium state vector by $\mathsf{s} := (\varepsilon_a\,,\ \varepsilon_b\,,\ \rho_L v_a\,,\ \rho_L v_b)^\mathsf{T}$, and further define $\mathsf{f} := -(v_a\,,\ v_b\,,\ P_{a1}\,,\ P_{b1})^\mathsf{T}$. We consider a grid of uniform length ΔX, and approximate the values of s and f as constants within each length element, where the i^{th} element is denoted using superscript i (Fig. 2). In order to formulate the finite volume method, we first find an approximate solution to the Riemann problem between two adjacent phases in cells i and $i+1$. To this end, we express the difference between $\mathsf{f}^{(i+1)}$ and $\mathsf{f}^{(i)}$ as

$$\mathsf{f}^{(i+1)} - \mathsf{f}^{(i)} = \sum_{n=1}^{2} [\![a_n]\!]^i\, \mathsf{r}_n^{(i)} + \sum_{n=3}^{4} [\![a_n]\!]^i\, \mathsf{r}_n^{(i+1)}; \tag{14}$$

here, $\{\mathsf{r}_n\}$ are the following eigenvectors of the matrix in Eq. (11)

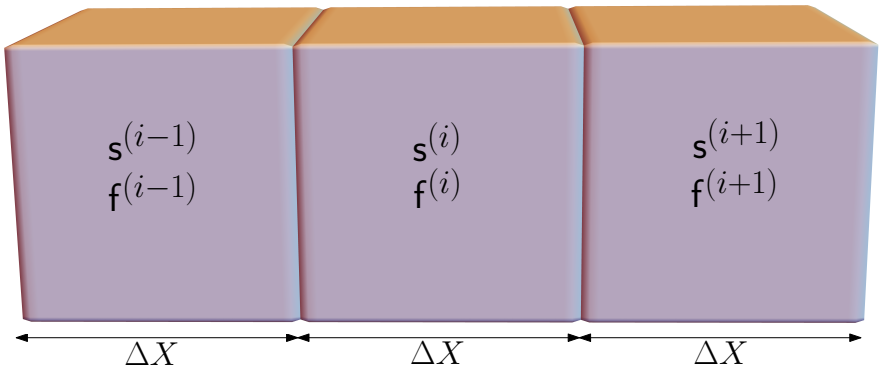

Figure 2: Illustration of the discretization of the material in the numerical scheme.

$$r_1 = \begin{pmatrix} 1 \\ \eta \\ \rho_L c_+ \\ \eta \rho_L c_+ \end{pmatrix}, \; r_2 = \begin{pmatrix} -\zeta \\ 1 \\ -\zeta \rho_L c_- \\ \rho_L c_- \end{pmatrix}, \; r_3 = \begin{pmatrix} -\zeta \\ 1 \\ \zeta \rho_L c_- \\ -\rho_L c_- \end{pmatrix}, \; r_4 = \begin{pmatrix} 1 \\ \eta \\ -\rho_L c_+ \\ -\eta \rho_L c_+ \end{pmatrix}, \tag{15}$$

where $\eta = -(\alpha - \rho_L c_+)/\beta$, $\zeta = \beta/(\alpha - \rho_L c_-)$, and $[\![a_n]\!]^i$ denotes the jump in f in the direction of its n^{th} eigenvector between cells i and $i+1$. Thus, Eq. (14) constitutes a linear algebraic system of equations for $[\![a_n]\!]^i$. Physically, this solution corresponds to four waves—two rightward and two leftward waves—propagating with the velocities $c_n = -c_+, -c_-, c_-$ and c_+, which contains jumps in f and s that are proportional to the respective eigenvectors. Characteristic curves as a representative solution to the Riemann problem of two adjacent phases in cells i and $i+1$ are shown in Fig. 3.

Note that the common approach in formulating finite volume methods is decomposing $\mathsf{s}^{(i+1)} - \mathsf{s}^{(i)}$ instead of $\mathsf{f}^{(i+1)} - \mathsf{f}^{(i)}$. In our problem the mismatch in the material parameters between the adjacent cells results in s containing an additional jump at the interface which is not in the direction of any of the eigenvectors. Since f must be continuous across the interface, we opt for expressing the difference in f, as presented in Eq. (14), which delivers in a simpler set of equations.

Next, we combine the approximate solution in a finite volume scheme, similarly to the approach of LeVeque (1997). We use a *Godunov-type* method with a second order correction (Godunov, 1959)

$$\mathsf{s}^{(i)}(t+\Delta t) = \mathsf{s}^{(i)}(t) - \frac{\Delta t}{\Delta X}\left(\mathsf{f}^{(i,i+1)} - \mathsf{f}^{(i-1,i)}\right) - \frac{\Delta t}{2\Delta X}\left(\hat{\mathsf{f}}^{(i,i+1)} - \hat{\mathsf{f}}^{(i-1,i)}\right), \tag{16}$$

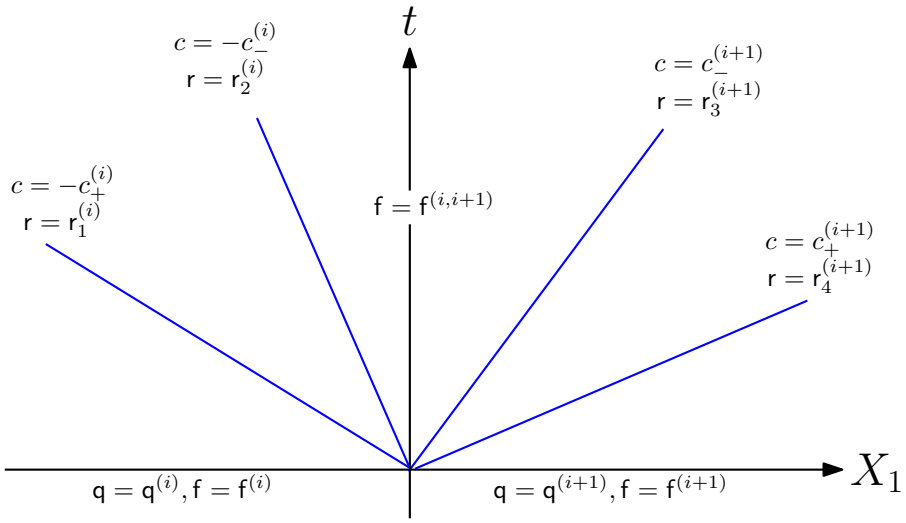

Figure 3: Representative characteristic curves associated with the solution to the Riemann problem of two adjacent phases between cells i and $i+1$.

where

$$\mathsf{f}^{(i,i+1)} := \mathsf{f}^{(i)} + [\![a_1]\!]^i \mathsf{r}_1^{(i)} + [\![a_2]\!]^i \mathsf{r}_2^{(i)} \equiv \mathsf{f}^{(i+1)} - [\![a_4]\!]^i \mathsf{r}_4^{(i+1)} - [\![a_3]\!]^i \mathsf{r}_3^{(i+1)} \tag{17}$$

is the value of f at the interface (see Fig. 3), and

$$\hat{\mathsf{f}}^{(i,i+1)} = \sum_{n=1}^{4} \operatorname{sign} c_n^{(i+j)} \left(1 - \frac{\Delta t}{\Delta X} \left| c_n^{(i+j)} \right| \right) [\![a_n]\!]^i \mathsf{r}_n^{(i+j)} \tag{18}$$

is the second order correction, with j equals 0 (resp. 1) for $n = 1,2$ (resp. $n = 3,4$).

While the second order correction improves the numerical solution when the exact solution is smooth, in case of discontinuities it may lead to unwanted numerical oscillations. To resolve this issue, we use a wave limiter (LeVeque, 1997), namely, we replace $[\![a_n]\!]^i$ in Eq. (18) by $\phi\left(\theta_n^{(i,i+1)}\right)[\![a_n]\!]^i$, where ϕ is a function of

$$\theta_n^{(i,i+1)} = \frac{c_n^{(i+j)}}{c_n^{(i-j+1)}} \frac{[\![a_n]\!]^{i-2j+1}}{[\![a_n]\!]^i} \frac{\mathsf{r}_n^{\mathsf{T}(i+j)} \cdot \mathsf{r}_n^{(i-j+1)}}{\mathsf{r}_n^{\mathsf{T}(i+j)} \cdot \mathsf{r}_n^{(i+j)}}. \tag{19}$$

The *monotonized centered* function is a simple example of ϕ, defined by

$$\phi = \max\left\{0, \min\left(\frac{1}{2} + \frac{\theta_n^{(i,i+1)}}{2}, 2\theta_n^{(i,i+1)}\right)\right\}. \tag{20}$$

Lastly, in order for the method to be numerically stable, it is necessary for the *CFL condition* to be satisfied, that is

$$\frac{\Delta t}{\Delta X}\max_i c_+^{(i)} < 1. \tag{21}$$

The left-hand side in Eq. (21) is referred to as the CFL number (Courant et al., 1967). The *domain of dependence* of a point $\{x_0,t_0\}$ is the set of points $\{x,t\}$ upon which the solution $u_i(x_0,t_0)$ has a dependency. The CFL condition ensures that the domain of dependence of the exact solution to the partial differential equation is contained within the domain of dependence of the numerical solution. If the CFL condition is not satisfied, then the exact solution depends on a larger set of points than the numerical solution. In such case, changing the state in certain points may change the exact solution but not the numerical solution, and therefore the numerical solution cannot converge to the exact one.

4 Application to Gentian layers

By way of example, we apply our method for phases governed by the compressible Gent model (Gent, 1996). The corresponding Gent strain energy density of phase n is

$$\Psi^{(n)}(\mathbf{F}) = -\frac{\mu^{(n)}J_m^{(n)}}{2}\ln\left(1-\frac{\mathrm{tr}\mathbf{F}^{\mathrm{T}}\mathbf{F}-3}{J_m^{(n)}}\right)-\mu^{(n)}\ln\det\mathbf{F}+\left(\frac{\kappa^{(n)}}{2}-\frac{\mu^{(n)}}{3}-\frac{\mu^{(n)}}{J_m^{(n)}}\right)(\det\mathbf{F}-1)^2, \tag{22}$$

where $\mu^{(n)}$ and $\kappa^{(n)}$ correspond to the shear and bulk moduli in the limit of small strains, respectively, and $J_m^{(n)}$ models the strain stiffening that rubber exhibits due to the limited extensibility of its polymer chains. This model—originally developed for capturing the strain stiffening of rubber at large strains—was recently shown useful by Ziv and Shmuel (2019a) for modeling shear shocks and tensile-induced shocks (Niemczura and Ravi-Chandar, 2011, Catheline et al., 2003, Espíndola et al., 2017).

We first study in Sec. 4.1 the scattering of an incident shock wave from one half-space, impinging on an interface with a second half-space made of a different material. Subsequently, in Sec. 4.2 we examine a two-phase laminate subjected to a strain pulse. In the numerical examples to follow, we choose $CFL = 0.9$.

4.1 Interface between two half-spaces

We consider the case of reflection and transmission of an incident shock wave at interface of two elastic half-spaces. This benchmark problem is chosen since we are able to obtain for it numerical solutions using standard root-finding algorithms—and specifically Newton's method—which will be compared with our finite volume method. We choose the exemplary model parameters

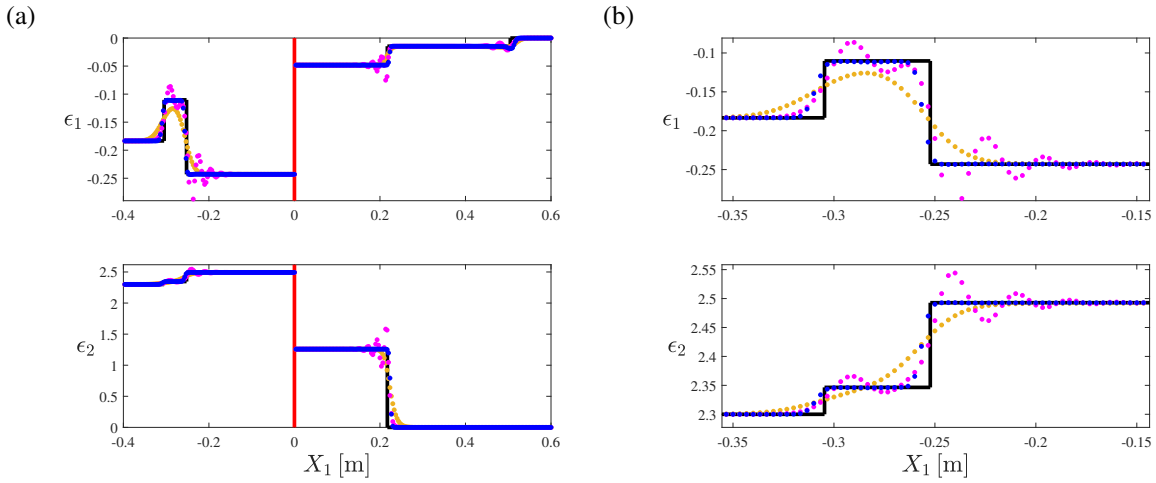

Figure 4: The distribution of ε_1 and ε_2 at $t = 10\,\text{ms}$ across (a) $-0.4\,\text{m} < X_1 < 0.6\,\text{m}$ and (b) $-0.35\,\text{m} < X_1 < -0.15\,\text{m}$ for the scattering problem of an incident shock wave from one half-space, impinging on the interface with a second half-space made of a different material. The pre-shock state is unstrained and at rest, and the post-shock state is $(\varepsilon_1, \varepsilon_2, v_1, v_2) \approx (-0.2, 2.3, 2.6, -32.4)$. The black line corresponds to the solution using Newton's method; orange, magenta and blue circles correspond to our finite volume solutions when $\phi = 0,\ 1$ and when ϕ is given by Eq. (20), respectively.

$$4\kappa^{(a)} = \kappa^{(b)} = 2\,\text{MPa},\ 4\mu^{(a)} = \mu^{(b)} = 400\,\text{kPa},\ J_m^{(a)} = J_m^{(b)} = 10,\ \rho_L^{(a)} = \rho_L^{(b)} = 1000\,\text{kg/m}^3. \quad (23)$$

Material a is subjected to a shock wave for which the pre-shock state is unstrained and at rest, and its post-shock state is $(\varepsilon_1, \varepsilon_2, v_1, v_2) \approx (-0.2, 2.3, 2.6, -32.4)$. These initial conditions were chosen to generate four shock waves, for which we obtain numerical solutions using Newton's method (Appendix A). We use a grid of 300 cells per meter and compare solutions using three different functions for ϕ in our scheme, namely, (i) $\phi = 0$; (ii) $\phi = 1$; and (iii) ϕ as given by Eq. (20).

Fig. 4a shows the distribution of ε_1 (upper panel) and ε_2 (lower panel) across $-0.4\,\text{m} < X_1 < 0.6\,\text{m}$ at $t = 10\,\text{ms}$. The black line corresponds to the numerical solution of the exact equations. The orange, magenta and blue circles correspond to finite volume solutions when $\phi = 0,\ 1$ and when ϕ is given by Eq. (20), respectively. Notably, all solutions obtained by the numerical scheme capture accurately the strain in the vicinity of the interface. Further, by comparing the three numerical solutions, we observe that the solution obtained with $\phi = 0$ qualitatively follows the numerical solution of the exact equations, but generally fails in recovering the discontinuities. Contrarily, the solution obtained with $\phi = 1$ captures the discontinuities better, albeit at the cost of oscillations in their vicinity. The solution obtained with the monotonized center limiter outperforms the previous solutions in capturing the shock waves accurately and without oscillations. To facilitate the observation of these features, we provide a zoom in of the region $-0.35\,\text{m} < X_1 < -0.15\,\text{m}$ in Fig. 4b.

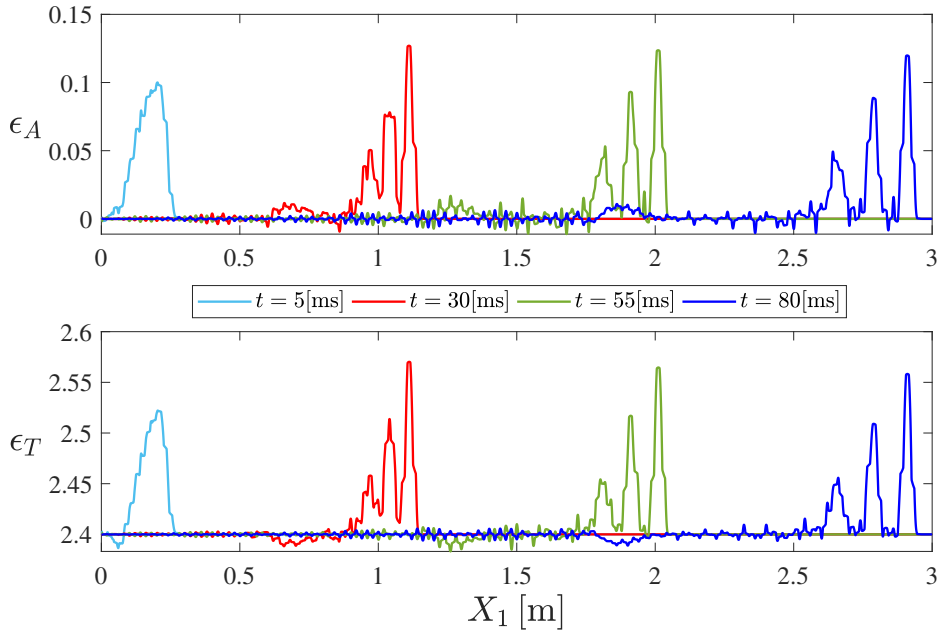

Figure 5: The strains ε_1 and ε_2 as functions of X_1 for a laminate with material parameters (24) and a grid of 2000 cells per meter. The prescribed initial state is given by Eq. (25) where $\varepsilon_1^{(I)} = 0$, $\varepsilon_2^{(I)} = 2.4$, $A_1 = A_2 = 0.2$, $L = 6\,\mathrm{m}$ and $w = 0.19\,\mathrm{m}$. Cyan, red, green and blue lines correspond to $t = 5\,\mathrm{ms}$, $30\,\mathrm{ms}$, $55\,\mathrm{ms}$ and $80\,\mathrm{ms}$, respectively.

4.2 Two-phase periodic laminates

We consider an infinite laminate composed of two alternating a and b Gent layers with an equal length of $h^{(a)} = h^{(b)} = 1\,\mathrm{cm}$, undergoing the motion (3). The model parameters of the layers are

$$\kappa^{(a)} = \kappa^{(b)} = 1\,\mathrm{MPa},\ \mu^{(a)} = \mu^{(b)} = 200\,\mathrm{kPa},\ J_m^{(a)} = J_m^{(b)} = 10,\ 8\rho_L^{(a)} = \rho_L^{(b)} = 4000\,\mathrm{kg/m^3}. \quad (24)$$

The laminate is subjected to the initial strain field

$$\varepsilon_i\,(X_1, t=0) = \begin{cases} \varepsilon_i^{(I)} + A_i \cos\frac{\pi}{w} X_1, & -\frac{w}{2} < X_1 < \frac{w}{2}, \\ \varepsilon_i^{(I)}, & \text{elsewhere}, \end{cases} \quad (25)$$

where $\varepsilon_i^{(I)}$, A_i and w are prescribed quantities, and the values of i depend on the type of displacements considered, as described next.

Coupled axial and transverse displacements.—Here, i takes the values 1 and 2, and we set $\varepsilon_1^{(I)} = 0$, $\varepsilon_2^{(I)} = 2.4$, $A_1 = A_2 = 0.2$ and $w = 0.19\,\mathrm{m}$.

Fig. 5 shows ε_1 and ε_2 as functions of X_1, using a grid of 2000 cells per meter. Cyan, red,

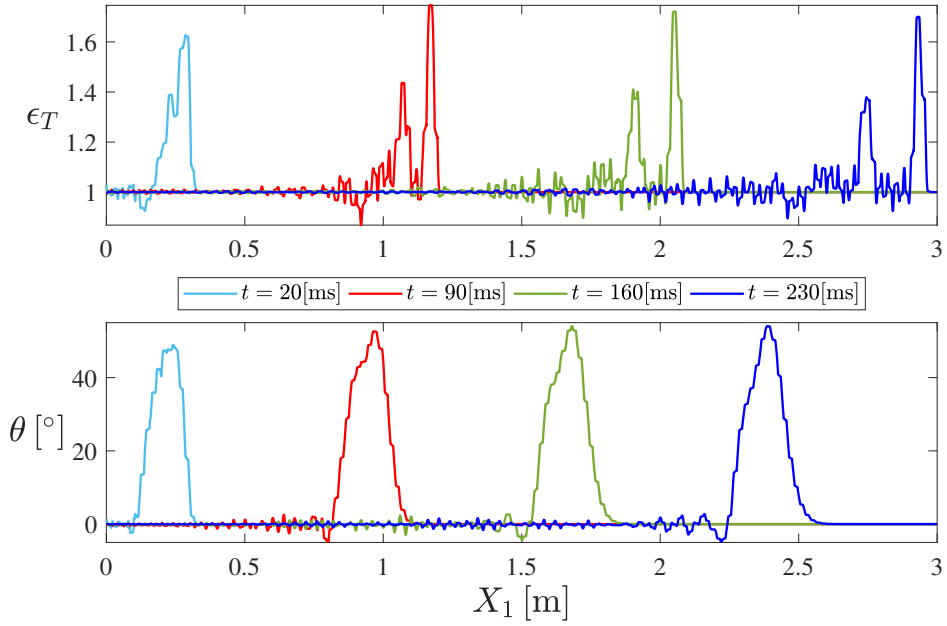

Figure 6: the distribution of ε_T and θ as functions of X_1 for a laminate with material parameters (24) and a grid of 2000 cells per meter. The prescribed initial state is given by Eq. (25) where $\varepsilon_2^{(I)} = 1$, $\varepsilon_3^{(I)} = 0$, $A_2 = 0$, $A_3 = 2$ and $w = 0.2\,\mathrm{m}$. Cyan, red, green and blue lines correspond to $t = 20\,\mathrm{ms}$, $90\,\mathrm{ms}$, $160\,\mathrm{ms}$ and $230\,\mathrm{ms}$, respectively.

green and blue lines correspond to $t = 5\,\mathrm{ms}$, $30\,\mathrm{ms}$, $55\,\mathrm{ms}$ and $80\,\mathrm{ms}$, respectively. Remarkably, the rightward propagating wave[1] is separated into a train of vector solitary waves, maintaining both their axial and shear components. This is the first report of such waves in soft laminates, thereby generalizing the pressure solitary waves in nonlinear laminates observed by LeVeque (2002), and establishing a continuum counterpart to the vector solitary waves in discrete systems reported recently by Deng et al. (2017, 2018, 2019b).

Coupled transverse displacements in two dimensions.—In this case $i = 2$ and 3, and we set $\varepsilon_2^{(I)} = 1$, $\varepsilon_3^{(I)} = 0$, $A_2 = 0$, $A_3 = 2$ and $w = 0.2\,\mathrm{m}$.

Fig. 6 shows ε_T and θ as functions of X_1, using a grid of 2000 cells per meter. Cyan, red, green and blue lines correspond to $t = 20\,\mathrm{ms}$, $90\,\mathrm{ms}$, $160\,\mathrm{ms}$ and $230\,\mathrm{ms}$, respectively. Notably, the field propagates as a train of linearly polarized solitary waves, followed by a single slower circularly polarized wave, which approximately maintain its shape.

[1] Owing to the symmetry of the problem, a mirrored wave that is propagating to the left is also generated.

5 Summary

We have developed a designated scheme to numerically solve the equations that govern elastic waves with two coupled components of finite amplitude in laminates made of nonlinear layers. Our method generalizes the approach of LeVeque (2002), who incorporated solutions for Riemann problems in finite volume schemes to solve the case where there is only an axial displacement. Our extension accounts for the generation of additional waves with respect to one-component problems, using a suitable matrix formulation which also captures the coupling between the different components of the displacement field. We have specifically addressed two cases, namely, a motion with coupling between its axial and transverse components, and a motion with two coupled transverse components.

The first application of our method was in a benchmark problem of an incident shock impinging on an interface between two half-spaces made of different materials. The constitutive response of the half-spaces is described by the Gent model, which was shown to capture experimental data of shear shock waves and tensile-induced shocks in soft materials. For this problem, numerical solutions using standard root-finding algorithms are accessible, and a comparison between such solutions using Newton's method and our method has shown an excellent agreement between the two solutions. Notably, the employment of a wave limiter in our scheme demonstrated a significant improvement of the results near discontinuities in the solution.

Our second application was for an initially strained periodic laminate made of two alternating Gent layers. In the case of coupled axial and transverse displacements, our method revealed the generation of vector solitary waves. This is the report of such waves in a continuum medium, *cf.* the report of vector solitary waves in discrete mechanical systems by Deng et al. (2017, 2018, 2019b). In the case of a coupling between two displacement components in the plane of the layers, our scheme revealed a single propagating circularly polarized wave that follows a train of linearly polarized solitary waves. The framework we developed offers a platform for a comprehensive study of these type of waves, to be pursued in a future work (Ziv and Shmuel, 2019b), as well as their extension to higher dimensional problems.

Acknowledgments

We acknowledge the support of the Israel Science Foundation, funded by the Israel Academy of Sciences and Humanities (Grant no. 1912/15), the United States-Israel Binational Science Foundation (Grant no. 2014358), and Ministry of Science and Technology (grant no. 880011).

Appendix A. Solution to a transmission problem between two half-spaces

The general solution to the interface problem formulated in Sec. 4.1 consists of four waves, namely, two leftward propagating waves and two rightward propagating waves. When the waves propagate as shocks, the jump conditions across each shock are (Davison, 1966)

$$\begin{aligned} \rho_L [\![v_1]\!] V + [\![P_{11}]\!] = 0, \; [\![\varepsilon_1]\!] V + [\![v_1]\!] = 0, \\ \rho_L [\![v_2]\!] V + [\![P_{21}]\!] = 0, \; [\![\varepsilon_2]\!] V + [\![v_2]\!] = 0, \end{aligned} \tag{A.1}$$

where $[\![\circ]\!]$ is the jump in $(\circ)$ ahead and behind the shock and V is the shock velocity. The continuity of the velocity and traction at the interface is

$$\begin{pmatrix} v_1^{(a)} \\ v_2^{(a)} \\ P_{11}^{(a)} \\ P_{21}^{(a)} \end{pmatrix} = \begin{pmatrix} v_1^{(b)} \\ v_2^{(b)} \\ P_{11}^{(b)} \\ P_{21}^{(b)} \end{pmatrix}. \tag{A.2}$$

Eqs. (A.1) and (A.2) yield 20 equations for determining 16 field variables and 4 shock velocities. The components v_1, v_2, P_{11}, and P_{21} are nonlinear functions of the deformation, hence closed-form solutions are not accessible. The numerical solution to the interface problem formulated in Sec. 4.1 is obtained with Newton's method using the commercial software Mathematica 11.3 (Wolfram Research, Inc.).

References

Jacob Aboudi and Yako Benveniste. One-dimensional finite amplitude wave propagation in a compressible elastic half-space. *International Journal of Solids and Structures*, 9(3):363 – 378, 1973. ISSN 0020-7683. doi: https://doi.org/10.1016/0020-7683(73)90086-3. URL http://www.sciencedirect.com/science/article/pii/0020768373900863.

Philip Trevor Barton, Dimitris Drikakis, and EI Romenski. An eulerian finite-volume scheme for large elastoplastic deformations in solids. *International journal for numerical methods in engineering*, 81(4):453–484, 2010.

Arkadi Berezovski and GA Maugin. Simulation of thermoelastic wave propagation by means of a composite wave-propagation algorithm. *Journal of Computational Physics*, 168(1):249–264, 2001.

Harold Berjamin, Bruno Lombard, Guillaume Chiavassa, and Nicolas Favrie. Plane-strain waves in nonlinear elastic solids with softening. *Wave Motion*, 89:65–78, 2019.

Katia Bertoldi, Vincenzo Vitelli, Johan Christensen, and Martin van Hecke. Flexible mechanical metamaterials. *Nature Reviews Materials*, 2(11):17066, 2017.

Olivier Bou Matar, Pierre-Yves Guerder, YiFeng Li, Bart Vandewoestyne, and Koen Van Den Abeele. A nodal discontinuous galerkin finite element method for nonlinear elastic wave propagation. *The Journal of the Acoustical Society of America*, 131(5):3650–3663, 2012. doi: 10.1121/1.3693654. URL https://doi.org/10.1121/1.3693654.

Michael M Carroll. Some results on finite amplitude elastic waves. *Acta Mech.*, 3(2):167–181, 1967.

S. Catheline, J.-L. Gennisson, M. Tanter, and M. Fink. Observation of shock transverse waves in elastic media. *Phys. Rev. Lett.*, 91:164301, Oct 2003. doi: 10.1103/PhysRevLett.91.164301. URL https://link.aps.org/doi/10.1103/PhysRevLett.91.164301.

Simon Chabot, Nathalie Glinsky, Enrique Diego Mercerat, and LF Bonilla Hidalgo. A high-order discontinuous galerkin method for 1d wave propagation in a nonlinear heterogeneous medium. *Journal of Computational Physics*, 355:191–213, 2018.

S. Chockalingam and T. Cohen. Shear shock evolution in incompressible soft solids. *Journal of the Mechanics and Physics of Solids*, 134:103746, 2020. ISSN 0022-5096. doi: https://doi.org/10.1016/j.jmps.2019.103746. URL http://www.sciencedirect.com/science/article/pii/S0022509619306684.

W D Collins. One-dimensional non-linear wave propagation in incompressible elastic materials. *The Quarterly Journal of Mechanics and Applied Mathematics*, 19(3):259–328, 1966.

Richard Courant, Kurt Friedrichs, and Hans Lewy. On the partial difference equations of mathematical physics. *IBM journal of Research and Development*, 11(2):215–234, 1967.

L Davison. Propagation of plane waves of finite amplitude in elastic solids. *Journal of the Mechanics and Physics of Solids*, 14(5):249–270, 1966. ISSN 0022-5096. doi: https://doi.org/10.1016/0022-5096(66)90022-6. URL http://www.sciencedirect.com/science/article/pii/0022509666900226.

Lee Davison. *Fundamentals of Shock Wave Propagation in Solids*. Springer-Verlag Berlin Heidelberg, 2008.

B Deng, J R Raney, V Tournat, and K Bertoldi. Elastic vector solitons in soft architected materials. *Phys. Rev. Lett*, 118:204102, 2017.

Bolei Deng, Pai Wang, Qi He, Vincent Tournat, and Katia Bertoldi. Metamaterials with amplitude gaps for elastic solitons. *Nature communications*, 9(1):3410, 2018.

Bolei Deng, Chengyang Mo, Vincent Tournat, Katia Bertoldi, and Jordan R Raney. Focusing and mode separation of elastic vector solitons in a 2d soft mechanical metamaterial. *Physical review letters*, 123(2):024101, 2019a.

Bolei Deng, Vincent Tournat, Pai Wang, and Katia Bertoldi. Anomalous collisions of elastic vector solitons in mechanical metamaterials. *Physical Review Letters*, 122:044101, 2019b.

Michel Destrade and Giuseppe Saccomandi. Finite amplitude elastic waves propagating in compressible solids. *Physical Review E*, 72(1):16620, 2005.

David Espindola and Gianmarco Pinton. Flash focus ultrasonic images sequences for shear shock wave observation in the brain. *The Journal of the Acoustical Society of America*, 141(5):3549–3549, 2017.

David Espíndola, Stephen Lee, and Gianmarco Pinton. Shear shock waves observed in the brain. *Physical Review Applied*, 8(4):044024, 2017.

Tiernan R Fogarty and Randall J LeVeque. High-resolution finite-volume methods for acoustic waves in periodic and random media. *The Journal of the Acoustical Society of America*, 106(1): 17–28, 1999.

A N Gent. A new constitutive relation for rubber. *Rubber Chem. Technol.*, 69:59–61, 1996.

Sergei Konstantinovich Godunov. A difference method for numerical calculation of discontinuous solutions of the equations of hydrodynamics. *Matematicheskii Sbornik*, 89(3):271–306, 1959.

Myungwon Hwang and Andres F Arrieta. Input-independent energy harvesting in bistable lattices from transition waves. *Scientific reports*, 8(1):3630, 2018.

Peter Lax and Burton Wendroff. Systems of conservation laws. *Communications on Pure and Applied mathematics*, 13(2):217–237, 1960.

Randall J LeVeque. *Numerical methods for conservation laws*, volume 132. Springer, 1992.

Randall J. LeVeque. Wave propagation algorithms for multidimensional hyperbolic systems. *Journal of Computational Physics*, 131(2):327 – 353, 1997. ISSN 0021-9991. doi: https:

//doi.org/10.1006/jcph.1996.5603. URL http://www.sciencedirect.com/science/article/pii/S002199919695603X.

Randall J LeVeque. Finite-volume methods for non-linear elasticity in heterogeneous media. *International journal for numerical methods in fluids*, 40(1-2):93–104, 2002.

N Nadkarni, C Daraio, and D M Kochmann. Dynamics of periodic mechanical structures containing bistable elastic elements: From elastic to solitary wave propagation. *Phys. Rev. E*, 90 (2):23204, 2014. doi: 10.1103/PhysRevE.90.023204. URL http://link.aps.org/doi/10.1103/PhysRevE.90.023204.

Neel Nadkarni, Andres F Arrieta, Christopher Chong, Dennis M Kochmann, and Chiara Daraio. Unidirectional transition waves in bistable lattices. *Physical review letters*, 116(24):244501, 2016.

J Niemczura and K Ravi-Chandar. On the response of rubbers at high strain rates—II. Shock waves. *Journal of the Mechanics and Physics of Solids*, 59(2):442–456, 2011. ISSN 0022-5096. doi: https://doi.org/10.1016/j.jmps.2010.09.007. URL http://www.sciencedirect.com/science/article/pii/S0022509610001833.

J Raney, N Nadkarni, C Daraio, D M Kochmann, J A Lewis, and K Bertoldi. Stable propagation of mechanical signals in soft media using stored elastic energy. *Proc. Natl. Acad. Sci. U. S. A.*, 2016.

PL Roe. Upwind schemes using various formulations of the euler equations. *Numerical Methods for the Euler equations of fluid dynamics*, pages 14–31, 1985.

Alexander M Samsonov, Irina V Semenova, and Fedor E Garbuzov. Nonlinear guided bulk waves in heterogeneous elastic structural elements. *International Journal of Non-Linear Mechanics*, 94:343–350, 2017.

Bharat B Tripathi, David Espíndola, and Gianmarco F Pinton. Modeling and simulations of two dimensional propagation of shear shock waves in relaxing soft solids. *Journal of Computational Physics*, 2019.

Wolfram Research, Inc. Mathematica 11.3. URL https://www.wolfram.com.

Hiromi Yasuda, Yasuhiro Miyazawa, Efstathios G Charalampidis, Christopher Chong, Panayotis G Kevrekidis, and Jinkyu Yang. Origami-based impact mitigation via rarefaction solitary wave creation. *Science advances*, 5(5):eaau2835, 2019.

Ron Ziv and Gal Shmuel. Smooth waves and shocks of finite amplitude in soft materials. *Mechanics of Materials*, 135:67 – 76, 2019a. ISSN 0167-6636. doi: https://doi.org/10.1016/j.mechmat.2019.05.002. URL http://www.sciencedirect.com/science/article/pii/S016766361930002X.

Ron Ziv and Gal Shmuel. Vector solitary waves in soft laminates. *In preparation*, 2019b.